ACTIVE CONTROL TO AUGMENT ROTOR LEAD-LAG DAMPING

Ch. Kessler, G. Reichert

Institute of Flight Mechanics
Technical University of Braunschweig, Germany

Abstract

Hingeless and bearingless rotor designs are today well accepted for modern helicopters. Continued development, however, revealed some deficiencies in the area of aeromechanical stability and vibration.
In general there is a good basic understanding how to avoid these instabilities. But since it becomes more and more desirable to focus rotor design on aerodynamic features and flight performance these aeromechanical instabilities gain new importance due to the difficulties to provide the required damping.

Since all rotor concepts suffer from the lack of sufficient natural lead-lag or inplane damping most designs in use show artificial lead-lag dampers to overcome aeromechanical instabilities. On the other hand, active control offers the possibility for an artificial stabilization of aeromechanical instabilities. Meanwhile, many research activities focus on active control to augment rotor lead-lag damping and many authors demonstrate the potential inherent in this approach.

The paper shortly repeats the problem of aeromechanical instabilities of hingeless rotor-systems. A simple rotor blade model with flap, lag and pitch DOFs is used to derive the coupled set of differential equations. The emphasis of this paper is to demonstrate the potential of active control and to gain physical understanding. The paper demonstrates lead-lag damping augmentation of an isolated rotor blade with lead-lag rate and attitude feedback even in forward flight. However, some problems are being discussed that may limit the success of an active control approach.

Notations and Abbreviations

a	blade hinge offset
$c = 2b$	blade chord
$C_{a\alpha}$	blade lift curve slope
C_{d0}	blade profile drag coefficient
C_{m0}	blade profile moment coefficient
C_T	thrust coefficient
$d_\beta, d_\zeta, d_\theta$	damping constants
D	fuselage drag force, damping ratio
f	fuselage parasite drag area
F	rotor thrust, force
G_{xi}	feedback gain for state variable x_i
h	offset of rotor hub from c.g.
I_{Bl}	flap and lag moment of inertia about hinge
I_θ	torsional moment of inertia about blade c.g.
$I_{B\theta}$	coupling moment of inertia
$k_\beta, k_\zeta, k_\theta$	flap, lag, torsion spring constants
k_x, k_y	coefficients of DREES inflow model
m_{Bl}, m_F	blade and fuselage mass
M_{Bl}	static blade moment of inertia
$\mathbf{Q}$	state vector weighting matrix
R	structural flap-lag coupling parameter
$\bar{R}$	rotor radius
$\mathbf{R}$	weighting matrix of control inputs
$\mathbf{u}$	vector of control inputs
v_n, v_t	velocities normal and tangential to the blade
V	forward speed
W	weight
$\mathbf{x}$	state vector
y_C	blade c.g. offset from elastic axis
y_L	blade a.c. offset from elastic axis
α_R	forward tilt of rotor disk in forward flight
β	flap angle
γ	blade Lock number
ε	small parameter
ζ	lead–lag angle
ϑ	blade control pitch angle
θ	blade torsional angle
Θ	total blade pitch angle $\Theta = \theta + \vartheta$
λ	inflow ratio $\lambda = \lambda_i + \lambda_{fs}$, eigen value
λ_i	induced inflow
λ_{fs}	free stream inflow
μ	advance ratio
σ	real part of an eigen value
ψ	blade azimuth angle
Ω	rotor rotational speed
ω	imaginary part of an eigen value
0, C, S	collective and cyclic parts of a trim value
nom	nominal
tr	trim value
$\dot{(\ )}$	$= \partial(\ )/\partial\psi$

1 Introduction

Since the introduction of hingeless rotor helicopters by MBB in the sixties much R&D effort has focused on these rotor types. As a consequent development of hingeless rotors bearingless rotors are entering helicopter service (EC 135, MDX Explorer). The main advantages of such rotor systems compared to articulated ones are mechanical simplification, reduced drag, weight, parts and maintenance costs,

higher moment capability, determined by the flapping stiffness and faster moment setup due to cyclic control inputs and therefore better handling qualities [1]. There are two successfully flown hingeless rotor concepts. The Boelkow-System makes use of elastic coupling effects, the other (WG 13) prevents these couplings [2, 3]. Important parameters in designing hingeless/bearingless rotors are blade flapping and lagging frequencies. Both rotor systems can be divided into two distinct groups depending on the inplane frequency: soft-inplane rotors with $\omega_\zeta/\Omega < 1$ and stiff-inplane rotors $\omega_\zeta/\Omega > 1$. Low inplane rotor loads can only be achieved by using soft-inplane rotors. As a consequence of this modern hingeless/bearingless rotors are designed as soft-inplane, but are susceptible to ground and air resonance [4, 5, 6, 7]. These phenomenon derives from the lead-lag motion. Because of the lagging motion the net c.g. of the entire rotor may shift out of the rotor axis and generates a rotating unbalance at the rotor head. This unbalance results in self-excited oscillations which may become unstable at some rotor speeds. The background of these oscillations is a coupling of the low frequency regressing lead-lag mode with body pitch or roll. In contrast to soft-inplane rotors stiff-inplane rotors may show a flap-lag or flap-lag-torsion instability of the rotor blade itself [8, 9, 10, 11]. To prevent these instabilities sufficient lead-lag damping has to be provided. This can be done either by adding dampers or by using structural damping and damping from aeroelastic couplings or by Active Control Technology (ACT) [12]. The introduction of Fly-by-Wire technology and digital control systems of future helicopter generations offers a broad range of different ACT concepts.

The enormous control power inherent in hingeless/bearingless rotor concepts makes feedback control an effective means of augmenting system stability. With this in mind several authors examined the possibilities of suppressing ground and air resonance by ACT using a conventional swash plate. Early work was done by YOUNG et al. [13]. Feedback of roll attitude and roll rate was effective in suppressing a ground and air resonance instability. A more detailed study was carried out by STRAUB and WARMBRODT [14]. Two mechanisms were mentioned to stabilize ground resonance: first, controlling body pitch and roll through flapping moments, secondly, augmenting lead-lag damping through CORIOLIS coupling with blade flapping. Scheduling feedback parameters was found out to maximize damping augmentation.
In a second paper, STRAUB [15] studied linear optimal control of a four bladed articulated rotor helicopter. The gains were obtained from the solving RICATTI's equation. Choosing appropriate feedback signals from this full state compensators resulted in sufficient lead-lag damping of the closed loop system throughout the considered rotor speed range.
TAKAHASHI and FRIEDMANN [16] studied active control of air resonance. Feedback of body states only resulted in poor lead-lag damping and in a destabilization of the progressing lead-lag mode.

On the other hand, today's helicopters reach more and more limits of their efficiency. To overcome these limits modern control technologies like Higher Harmonic Control (HHC) and Individual Blade Control (IBC) are being discussed. Initially, the intension of HHC was to reduce vibration levels and to reach a jet smooth ride with vibration levels of about $0.02g$. Recent studies show that HHC can also lower rotor noise and required power [17, 18]. A more general extension of HHC is IBC. Each rotor blade is controlled independently of the others. This requires actuators and sensors for each blade in the rotating system. Since IBC includes HHC, IBC seems to be a promising control concept to solve most of the problems of future helicopters. Important work was done by N.D. HAM and R.M. MCKILLIP [19, 20, 21, 22, 23, 24]. The applications of IBC were investigated analytically as well as experimentally with a single bladed wind tunnel model. At present, the companies EUROCOPTER DEUTSCHLAND and ZF-LUFTFAHRTTECHNIK are working on an incorporation of IBC in helicopters. Flight and wind tunnel testing at NASA-Ames Research Center was done with a Bo 105 helicopter [25, 26]. The different purposes of IBC are:

- gust alleviation,
- blade stall suppression,
- vibration and noise reduction,
- blade bending stress limitations,
- flapping stabilization at high advance ratios and

- lead-lag damping augmentation.

Regarding this, REICHERT and ARNOLD [27] picked up the idea of controlling ground resonance through a conventional swash plate and compared these results with an IBC approach. The four bladed hingeless rotor was modelled similar to [14]. The IBC principle resulted in poor aeromechanical stability for the instable pitch mode compared to body pitch feedback results.

The aim of this paper is to discuss the use of IBC to augment rotor lead-lag damping in hover and forward flight. Therefore, an isolated rotor blade is considered and rotor body couplings are neglected. This considerably reduces model complexity and improves physical inside. Body dynamics will be included in further research activities.

2 Mathematical Model

The 3DOF flag-lag-torsion model of the hingeless rotor blade can be seen in fig. 1. The blade is assumed rigid rotating against linear springs and dampers about a

common hinge located a distance a out of the rotor axis. The hinge sequence is lead-lag inboard, flap and torsion outboard. The flap deflection β is positive up, lead-lag ζ positive forward (in direction of rotation) and torsion θ is positive nose up. The nonrotating rotor coordinate system (index Ro) is located in the rotor hub a distance h about the helicopter's centre of gravity. The z-axis along the rotor shaft is positive up and the x-axis opposite to the forward speed V. All other coordinate systems are located in the equivalent hinge with their x-axis pointing along the elastic axis and the z-axis upwards. The blade profile aerodynamic centre L and centre of gravity have an offset y_L and y_C respectively to the elastic axis E.

The differential equations are being derived by applying D' Alembert's principle. To reduce the complexity of the final equations and to retain only the important terms an ordering scheme is used [16, 28]. The ordering scheme is based on the assumption that

$$O(1) + O(\varepsilon^2) \approx O(1) \tag{1}$$

which states that terms of order ε^2 are negligible compared to terms of order unity. The quantity ε is a non-dimensional parameter which quantifies the meaning of a small parameter. A quantity is meant to be small, if it reaches values between $0.1 < \varepsilon < 0.2$. The assigned orders of magnitude of the important quantities used in this study are:

$$O(1) \quad : \quad \sin\psi,\ \cos\psi,\ \cos\vartheta,\ M_{Bl},\ I_{Bl},\ \ddot{\vartheta}_k,$$

$$O(\varepsilon^{\frac{1}{2}}) \quad : \quad \sin\vartheta,\ \vartheta,\ \dot{\vartheta},$$

$$O(\varepsilon) \quad : \quad \beta,\ \dot{\beta},\ \ddot{\beta},\ \zeta,\ \dot{\zeta},\ \ddot{\zeta},\ \theta,\ \dot{\theta},\ \ddot{\theta},\ c,\ b,\ \lambda,\ a,\ \alpha_R,$$

$$O(\varepsilon^{\frac{3}{2}}) \quad : \quad \frac{C_{d0}}{C_{a\alpha}},\ \frac{C_{m0}}{C_{a\alpha}},$$

$$O(\varepsilon^2) \quad : \quad y_C,\ y_L,\ I_{B\theta},\ g,$$

$$O(\varepsilon^{\frac{5}{2}}) \quad : \quad I_\theta.$$

The systematic application of this ordering scheme in the derivation procedure yields a consistent set of nonlinear equations of motion. The equations are:

flap equation:

$$
\begin{aligned}
I_{Bl}\ddot{\beta} \ &+\ [k_\beta + (k_\zeta - k_\beta)\sin^2(R\cdot\vartheta) + I_{Bl} + aM_{Bl}]\beta \\
&+\ d_\beta\dot{\beta} + 2I_{Bl}\beta\dot{\zeta} + y_C M_{Bl}(\ddot{\Theta}\cos\Theta + \sin\Theta) \\
&+\ [(k_\zeta - k_\beta)\sin(R\cdot\vartheta)\cos(R\cdot\vartheta)]\zeta \\
&+\ M_{Bl}g\cos\alpha_R + M_\beta\ =\ 0, \tag{2}
\end{aligned}
$$

lead-lag equation:

$$
\begin{aligned}
-I_{Bl}\ddot{\zeta} \ &+\ [-k_\zeta + (k_\zeta - k_\beta)\sin^2(R\cdot\vartheta) - aM_{Bl}]\zeta \\
&-\ d_\zeta\dot{\zeta} + 2I_{Bl}\beta\dot{\beta} + y_C M_{Bl}\ddot{\Theta}\sin\Theta \\
&-\ [(k_\zeta - k_\beta)\sin(R\cdot\vartheta)\cos(R\cdot\vartheta)]\beta \\
&+\ M_{Bl}g\sin\alpha_R\sin\psi + M_\zeta\ =\ 0, \tag{3}
\end{aligned}
$$

torsion equation:

$$
-I_\theta(\ddot{\Theta} \ +\ \cos\Theta\sin\Theta) - k_\theta\theta - d_\theta\dot{\theta}
$$

$$
\begin{aligned}
&+\ y_C M_{Bl}(-\beta\cos\Theta - \ddot{\beta}\cos\Theta + \ddot{\zeta}\sin\Theta) \\
&-\ y_C g(\cos\alpha_R\cos\Theta + \sin\alpha_R\sin\Theta\sin\psi) \\
&+\ M_\Theta\ =\ 0, \tag{4}
\end{aligned}
$$

where $\Theta = \theta + \vartheta$ is the total pitch angle of the blade and R the structural coupling parameter. Two cases can be considered. $R = 0$ represents a rotor-hub configuration in which the blade is rigid and all the flexibility is concentrated in the hub. No structural coupling appears between flapping and lagging motion (WG 13). $R = 1$ idealizes a flexible blade with a rigid hub. Flap and lead-lag DOF are coupled (Bo 105). No intermedia values are valid. Thus, this representation is a simplified form of the well known rotor blade model given in [8, 9, 29]. The M_β, M_ζ, M_Θ are the aerodynamic pitch, flap and lag moments, respectively. They are derived from using a quasi-steady approximation of Greenberg's unsteady theory for low reduced frequencies in which the lift deficiency function is taken to be unity. This agrees with [10, 30]. These aerodynamic moments are:

$$M_\Theta \ =\ \int_0^{1-a} (dM_\Theta + dM_{\Theta 0}), \tag{5}$$

$$M_\beta \ =\ \int_0^{1-a} -x_P\,dF_\beta, \tag{6}$$

$$M_\zeta \ =\ \int_0^{1-a} x_P\,dF_\zeta \tag{7}$$

where dM_Θ, dF_β, dF_ζ are the differential pitching moment and forces acting at the blade section. Greenberg's theory is derived for a symmetric airfoil. As a crude adjustment, $dM_{\Theta 0}$ is added to equation (5), which accounts for a moment due to any camber in the airfoil cross-section. These differential moments and forces are given by

$$dF_\beta \ =\ \delta\left[-\frac{b}{2}P\sin\Theta + v_t Q - \frac{C_{d0}}{C_{a\alpha}}v_t^2\right]dx_P, \tag{8}$$

$$dF_\zeta \ =\ \delta\left[\frac{b}{2}P\cos\Theta - v_n Q - \frac{C_{d0}}{C_{a\alpha}}v_n v_t\right]dx_P, \tag{9}$$

$$
\begin{aligned}
dM_\Theta \ =\ \delta\Bigg[&\left(y_L - \frac{b}{2}\right)\frac{b}{2}P + \left(\frac{b^2}{4}\dot{\Theta} - y_L Q\right)v_t \\
&-\frac{b^3}{16}\dot{\Theta}\Bigg]dx_P, \tag{10}
\end{aligned}
$$

$$dM_{\Theta 0} \ =\ 2\delta\frac{C_{m0}}{C_{a\alpha}}bv_t^2\left[1 + \left(\frac{v_t}{v_n}\right)^2\right]dx_P, \tag{11}$$

where the following abbreviations are used:

$$\delta \ =\ \frac{1}{2}I_{Bl}\gamma, \tag{12}$$

$$P \ =\ \dot{v}_n - v_t\dot{\Theta} - \dot{v}_t\Theta + \left(\frac{b}{2} - y_L\right)\ddot{\Theta}, \tag{13}$$

$$Q \ =\ v_n - v_t\Theta + (b - y_L)\dot{\Theta}. \tag{14}$$

The dimensionless velocities normal v_n and tangential v_t to the blade section are:

$$v_t = -(a + x_P\zeta + x_P)$$
$$- \mu\zeta\cos\psi - \mu\sin\psi + O(\varepsilon^2), \qquad (15)$$

$$v_n = -(\lambda + x_P\dot{\beta})$$
$$- \mu\beta\cos\psi + \mu\beta\zeta\sin\psi + O(\varepsilon^3), \qquad (16)$$

where $\lambda = \lambda_{fs} + \lambda_i = \mu\tan\alpha_R + \lambda_i$. No reverse flow is considered. To adapt the induced inflow λ_i to the forward flight condition a linear variation of the inflow distribution over rotor disk is considered

$$\lambda_i = \lambda_{i0}(1 + k_x r\cos\psi + k_y r\sin\psi), \qquad (17)$$

where λ_{i0} is the mean induced inflow given by momentum theory in forward flight

$$\lambda_{i0} = \frac{C_T}{2\sqrt{\mu^2 + (\lambda_{fs} + \lambda_{i0})^2}} \qquad (18)$$

and k_x and k_y are constants taken from DREES's model [31]

$$k_x = \frac{4}{3}\left[(1 - 1.8\mu^2)\sqrt{1 + \left(\frac{\lambda}{\mu}\right)^2} - \frac{\lambda}{\mu}\right], \qquad (19)$$

$$k_y = -2\mu. \qquad (20)$$

From equation (19) and (20) it follows that both constants are zero in hover $\mu = 0$. k_x has a maximum of about 1.1 at $\mu = 0.16$ and is approximately 1 at $\mu \approx 0.3$.

3 Trim and Stability Solution

For stability analysis, it is convenient to write equations for small perturbation motions about a periodic equilibrium motion of the nonlinear system. Propulsive trim is used to compute the free flight equilibrium solution. That requires the calculation of pilot settings $\vartheta_0, \vartheta_C, \vartheta_S$ as well as the vehicle motion and orientation for a prescribed flight condition. This study is restricted to level flight. For a specified weight W and a given forward speed μ fifteen unknowns are evaluated: $\vartheta_0, \vartheta_C, \vartheta_S, \theta_0, \theta_C, \theta_S, \beta_0, \beta_C, \beta_S, \zeta_0, \zeta_C, \zeta_S, \lambda_{i0}, \alpha_R$ and k_x. Thus, fifteen equations are needed. These are nine rotor equilibrium equations. In simplified form they are:

$$\frac{1}{2\pi}\int_0^{2\pi}(\text{flap, lag, torsion equation})\,d\psi = 0,$$

$$\frac{1}{\pi}\int_0^{2\pi}(\text{flap, lag, torsion equation})\cos\psi\,d\psi = 0,$$

$$\frac{1}{\pi}\int_0^{2\pi}(\text{flap, lag, torsion equation})\sin\psi\,d\psi = 0.$$

For the inflow equation (18) and (19) have to be regarded. Finally, four overall equations for the helicopter are needed to trim the vehicle. These four equations are vertical and longitudinal force equilibrium as

well as pitch and roll moment equilibrium. The forces acting at the fuselage are the drag

$$D = \frac{1}{2}\frac{I_{Bl}}{C_{a\alpha}}\gamma f \mu^2$$

and the weight

$$W = m_F g$$

where g is the dimensionless earth gravity. Since the fuselage c.g. is located a distance h below the rotor hub centre and since no bank angle is trimmed both forces generate a pure pitching moment at the rotor centre:

$$M_F = W h \sin\alpha_R - D h \cos\alpha_R.$$

These fuselage forces and moment have to balance with the rotor forces and moments summed up over all rotor blades. For trim to be established, it is only necessary to satisfy the constant components of the four fuselage equilibrium equations. The harmonic components are associated with the vibratory loads and are not part of trimming the vehicle.

Linearizing about the equilibrium solution and transforming the three rotor blade differential equations into state space representation yields the well known equation:

$$\dot{\mathbf{x}} = \mathbf{A}(\psi)\mathbf{x} + \mathbf{B}(\psi)\mathbf{u}. \qquad (21)$$

The state vector $\mathbf{x}$ includes the six states $\dot{\theta}, \dot{\beta}, \dot{\zeta}, \theta, \beta, \zeta$ and the control vector $\mathbf{u}$ the control ϑ only. $\mathbf{A}(\psi)$ is the 2π-periodic system matrix and $\mathbf{B}(\psi)$ is the 2π-periodic control matrix. The periodicity vanishes in hover $\mu = 0$. Since both matrices are periodic in forward flight ($\mathbf{B}(\psi)$ is needed for latter control studies) FLOQUET theory has to be applied to examine system stability [31]. For this the FLOQUET transition matrix is computed numerically using a fourth order RUNGE-KUTTA procedure. The eigen values of the transition matrix are the characteristic multipliers. With these characteristic multipliers the characteristic exponents $\lambda = \sigma + j\omega$, $j = \sqrt{-1}$ can be calculated. The system is stable, if for all eigen values $\sigma < 0$ holds. Two problems arise from this theory:
1) Usually, the imaginary part ω of an eigen value can be worked out except an integer multiple of 1. In hover the system matrices show constant coefficients and the eigen values can be computed directly from the system matrix $\mathbf{A}$ (open or closed loop case). Since the imaginary part must change smoothly with increasing μ the right eigen frequency can be figured out from the hover value.
2) Constant coefficient systems show eigen values that are real or complex conjugated. For a helicopter in forward flight this is not necessarily true. For large advance ratios μ or large gains of the closed loop system a former complex conjugated eigen value pair breaks up into two different complex eigen values [31]. If the

$\bar{R}$	4.9m	$\bar{\Omega}$	44.5/s
N_{Bl}	4	$C_{a\alpha}$	5.9
I_{Bl}	0.333	C_{d0}	0.01
M_{Bl}	0.5	C_{m0}	-0.02
$\bar{m}_{Bl}$	23.4kg	γ	5.0
I_θ	0.0002	ω_β	1.15
a	0.15	ω_ζ	0.67
c	0.055	ω_θ	3.2
y_C	0.0	y_L	0.0
d_β	0.0	d_ζ	0.0
d_θ	0.0	$\bar{\rho}$	1.0kg/m³
h	0.3	$\bar{m}_F$	2006.4kg
f	0.8	$\bar{g}$	9.81m/s²

Table 1: Data of Nominal Configuration

advance ratio is limited to typical values of conventional helicopters and if the feedback gains are limited to moderate magnitudes in forward flight this problem does not arise.

The data used in this study correspond to a four bladed soft-inplane helicopter somewhat similar to the ECD Bo 105. The data of the nominal configuration are listed in Table 1. Non-dimensionless parameters can be distinguished from dimensionless ones by the bar $(\bar{\ })$.

Fig. 2 shows the trim solution of all trim values including k_y. The trim solution is calculated iteratively from nonlinear equilibrium equations using a NEWTON method. No small angle assumptions are introduced. Since all angles are plotted in degree units, the left ordinate is valid for the trim angles, whereas the right ordinate shows the dimensionless values for the inflow parameters λ, k_x, and k_y. According to the power required curve of a helicopter in forward flight, the collective control angle ϑ_0 starts at a relative high value in hover of about 11° and drops to its minimum at $\mu \approx 0.14$ before increasing again. For large advance ratios μ the shaft has to tilt more to compensate for the increase in parasite drag. Thus, the free stream inflow $\lambda_{fs} = \mu \tan \alpha$ also increases with increasing μ. Compared to this, the mean induced inflow λ_{i0} decreases with increasing μ. For high advance ratios λ_{i0} decreases almost inversely proportional with μ. Adding both curves yield the total inflow λ which shows the same characteristic nature as ϑ_0. The longitudinal inflow constant k_x shows the characteristics mentioned above. k_y decreases with a slope of "−2". To tilt the rotor shaft more with increasing advance ratio rotor pitching moments are needed. They are primarily generated by β_C which can be thought as a longitudinal tilt of the rotor tip path plane [31]. Thus, β_C slightly increases with forward speed, but the val-

Eigen Mode	$R = 0$		$R = 1$	
	σ	ω	σ	ω
θ	-0.27440	3.13233	-0.27442	3.13216
β	-0.20354	1.13639	-0.20254	1.13858
ζ	-0.00266	0.67014	-0.00366	0.66617

Table 2: Eigen Values in Hover

ues remain small. This forward tilt of the tip path plane or rotor shaft axis is established by negative longitudinal cyclic feathering ϑ_S. Since no side force equilibrium is considered no side-ward tilt of the rotor disk is needed to compensate the tail rotor thrust, for example. Therefore, β_S and ϑ_C are small. The collective flapping angle β_0 is almost constant versus μ, but ζ_0 shows an inverse characteristic of the ϑ_0 curve. This is a direct consequence of the drag at the rotor blade which varies with varying collective pitch.

These trim solutions agree well with theory and are qualitatively in close correlation with those from ref. [9] or [30]. The other values cannot be checked with literature, since both mentioned references do not show results for those variables.

Fig. 3 shows the real part σ_ζ of the lead-lag mode with ($R = 1$) and without ($R = 0$) structural flap-lag coupling. The lead-lag motion is weakly damped, whereas the other two motions are well damped and do not need to be considered further. To give an idea of the magnitudes, table 2 shows the hover values for the three eigen modes.

As can be seen from fig. 3 and table 2 the system is stable within the whole flight regime. Usually, flap-lag-torsion instabilities become a problem to stiff-inplane rotor helicopters [9]. The structural coupling parameter R has a stabilizing influence on lead-lag damping. For $R = 1$ the lead-lag mode is slightly more damped compared to $R = 0$ and the flapping mode is less damped. The structural coupling between flap and lag motion shifts damping from flap towards lead-lag. But the differences are small for the soft-inplane rotor. This behaviour of soft-inplane hingeless rotor configurations is known from many studies, e.g. [8, 9, 10]. The curve's characteristic again corresponds to the power required curve. The lead-lag damping starts at a moderate value in hover. Since stability was determined in the rotating reference frame the curve starts with a horizontal tangent in hover, compare [8, 32]. From that hover result σ_ζ decreases to a minimum value at $\mu \approx 0.16$ before increasing for advance ratios beyond this value. Since the case without structural coupling shows less damping compared to $R = 1$, structural flap-lag coupling is not considered for the active control studies.

3 Active Control to Augment Rotor Lead-Lag Damping

In the following paragraph possibilities and mechanisms of controlling the lead-lag motion will be discussed. A better understanding of the internal structure of rotor dynamics may help to interpret the influence of certain design parameters and to assess the effectiveness of feasible control loops.

Although this study considers an isolated rotor first, the aim of this research activity is to guarantee ground and air resonance stability by an IBC device. Several companies are engaged in developing actuators located above the swash plate to control blade pitch. Primary objective of the R&D effort is the realization of HHC to reduce vibration and noise levels. As soon as such actuators become reliable and available the extension to further control tasks seems to be practicable. The implementation of an air and ground suppression device would not be a problem as the required actuator bandwidth is well below those needed for HHC [27].

The feasible concepts to overcome ground or air resonance are summarized in fig. 4. Furthermore, the figure shows a general schematic of rotor body interaction. All active control approaches are changing blade pitch to control the degrees of freedom involved in ground and air resonance. As mentioned by STRAUB and WARMBRODT [14] two control paths exist: First, the fuselage pitch and roll motion can be controlled through rotor pitching and rolling moments arising from flapping. The magnitude of each is directly related to the equivalent blade root hinge offset and flap spring stiffness. This approach affords cyclic control inputs to generate cyclic flapping. Secondly, lead-lag damping augmentation can be achieved through CORIOLIS coupling with blade flapping. According to [14] this requires either steady blade coning deflection or built-in precone. Another mechanism to control lagging motion arises from the differential equations of motion. The rotor inplane aerodynamic forces contribute to blade lead-lag control. Ref. [27] clearly states that the lead-lag control efficiency through aerodynamic forces is of the same magnitude as the efficiency through CORIOLIS forces. Both effects have to be considered in an IBC study. Thus, both mechanisms are included in fig. 4. The kernel of this figure are the rotor dynamics. Torsion is not considered in this figure. From blade pitch input lift, drag and CORIOLIS forces generating flapping and lagging motion arise. Transformed into the non-rotating frame both motions result in collective and cyclic flap or lead-lag. These multiblade degrees of freedom cause body motions which have a direct impact on the rotor blade motion, and vice versa.

The first possibility to control a growing aeromechanical instability arises, if fuselage states such as roll or pitch rate are feed back to the cyclic control inputs. Such means are common standard in many modern helicopters and are designated as Stability Augmentation Systems (SAS). In general their purpose is to improve stability and handling qualities. Several authors examined the impact of a SAS on handling qualities and rotor dynamics with respect to different model complexities [33, 34]. On extending the bandwidth up to the frequency range which is relevant for air or ground resonance, it becomes possible to expand the task of SAS to suppression of aeromechanical instabilities. The advantage of such a device is obvious. Since the whole control system is located in the non-rotating frame, many parts of a classical SAS hardware can be used. Many studies demonstrated successfully an air and ground resonance suppression with such a control approach. In addition to the body states rotor states transferred into the non-rotating frame by introducing multiblade coordinates can be used to augment system stability [7, 14, 27]. In these studies the closed loop system was considerably stabilized although adverse effects like a destabilization of high frequency lead-lag modes or a worsening of handling qualities occur with increasing gains. These disadvantages can be avoided by inclusion of filters into the feedback loop.

The other control approach mentioned above is IBC. Lead-lag states or similar signals like blade root bending moments are measured in the rotating frame and are feed back individually for each blade to its control pitch input. Lead-lag augmentation has already been demonstrated theoretically and experimentally by HAM et al. [24]. REICHERT and ARNOLD [27] picked up the idea of controlling ground resonance by means of IBC and compared this to a conventional SAS approach. The IBC principle resulted in poor aeromechanical stability. In contrast to that, the SAS results were quite satisfying. Moreover, some restrictions in optimizing an IBC system were detected which will be discussed in a later chapter. Before this, IBC of an isolated rotor in forward flight will be studied in more detail.

If all states of a helicopter model are feed back one comes to full state feedback. Full state feedback is often called optimal control theory. Compared to all other control approaches, full state feedback yields theoretically the best results, but the control gains are limited for practical reasons. The gains are analytically determined by solving the matrix RICCATI equation [15]. The full state feedback formulation requires knowledge of all rotor, body and maybe inflow states (dynamic inflow). If all the states are accurately measured and if controllability is assured, the closed loop system possesses guaranteed stability and robust properties. However, as the fidelity of plant models continue to increase, all the states must be measured reliably. This is impractical. Therefore, observer based designs may be used to estimate any unmeasured states. If an observer is applied to a real, complex system (as the helicopter is) severe problems

may arise, since the observer needs a model of the plant. Such a model is difficult to realize. Furthermore, the closed loop system may be sensitive to certain inaccuracies of the observer model.

3.1 Lag Damping Augmentation in Hover

First, active control to augment rotor lead-lag damping shall be considered in hover, since all the periodicity vanishes for $\mu = 0$. With the linear equations of motion derived, so-called signal flow diagrams can be drawn. These diagrams help to illustrate the physical relations of a system and are widely used in control theory. Each state is assigned to an integrator and each state equation is fulfilled at the integrator's input. Fig. 5 displays the simplified signal flow diagram for the isolated rotor blade in hover. It is simplified, since only important couplings between the three rotor blade DOFs are considered. If, at first, the lead-lag motion is treated independently from flapping and torsional motion, the active control results of a 1DOF second order oscillator can be transferred to the lead-lag motion. From that it is known that feedback of rate increases damping and feedback of attitude changes the system stiffness. The three derivatives necessary to get the right sign of feedback gains to stabilize the lead-lag motion are

$$N_{\dot{\zeta}} = -\frac{d_\zeta}{I_{Bl}} - \gamma \frac{C_{d0}}{C_{a\alpha}} - \frac{\gamma}{2}\lambda_{i0}Q_{20}(\theta_0 + \vartheta_0), \qquad (22)$$

$$N_\zeta = -\frac{1}{I_{Bl}}\left(k_\zeta + a\,M_{Bl} + R(k_\beta - k_\zeta)\sin^2\vartheta_0\right)(23)$$

$$N_\vartheta = -\frac{\gamma}{2}\lambda_{i0}(Q_{20} + a\,Q_{10}) \qquad (24)$$

where

$$Q_{n0} = \int_0^{1-a} x_p^n \, dx_p . \qquad (25)$$

If lead-lag rate and angle are feed back to the control input ϑ the derivatives of the closed loop system are

$$N_{\dot{\zeta},cl} = N_{\dot{\zeta}} - G_{\dot{\zeta}}N_\vartheta, \qquad (26)$$

$$N_{\zeta,cl} = N_\zeta - G_\zeta N_\vartheta. \qquad (27)$$

From equation (26) it is immediately clear that $G_{\dot{\zeta}}$ must be less than zero. Since stiff-inplane rotors are prone to aeroelastic rotor blade instabilities, the system stiffness of the closed loop system should not be increased. Thus, G_ζ must be larger than zero which means a further softening of the rotor blade.

Of course, the treatment of the isolated lead-lag motion is a quite rough approximation of the problem. More detailed investigations have to consider the coupling with the flapping motion via N_β (CORIOLIS force) and N_β (structural coupling). Since the only control input is the blade pitch input ϑ and since a change of blade pitch excites torsion and flap this has a direct impact on lead-lag motion. From the active

control point of view a surface to control lead-lag motion only, like drag control, would be favourable. The following active control results have to show, if these simple considerations were right.

The root locus for lag rate (left) and lag angle (right) feedback are shown in fig. 6. The gains were varied between $-\infty < G_{\dot{\zeta}} \leq 0$ for lag rate and $-\infty < G_\zeta \leq 0$ and $0 \leq G_\zeta < \infty$ for lag attitude feedback, respectively. As known from the root locus theory the open loop poles × move into the zeros ⊙ of the transfer function for increasing gain. All remaining poles move towards infinity. From the left hand side of the figure it can be seen that small lead-lag rate gains $G_{\dot{\zeta}}$ actually increase lead-lag damping whereas the change of lead-lag frequency is small. Since a zero occurs right beside the torsion eigen value, this motion is not affected for the given range of $G_{\dot{\zeta}}$. But, as an adverse affect flap frequency decreases. This has to be avoided. A change of flapping frequency has a direct consequence for the handling qualities. For increasing gain the lead-lag eigen value moves in a circular arc towards the real axis. The corresponding eigen value of the upper and lower complex plain match at the real axis. Whereas the one eigen value moves into the zero in the origin of the complex plain the other moves on the real axis towards minus infinity. Because a zero occurs in the right hand plane, the flapping motion becomes unstable for $G_{\dot{\zeta}} = -16.9$. Of course this gain is much too high and will not be reached for practical purposes.

If lag attitude is feed back with $G_\zeta \geq 0$ the lead-lag eigen value moves almost parallel to the imaginary axis towards the real axis. There it breaks up into two real eigen values where the one crosses the imaginary axis for $G_\zeta = 14.4$, since no more zero lies in the origin. While the lagging frequency is changed by lead-lag feedback flapping frequency remains almost unchanged for $G_\zeta \geq 0$. The flap eigen value is shifted parallel to the real axis into the right complex plane and becomes unstable for $G_\zeta = 30.1$. Again, the torsion eigen value does not change much. For $G_\zeta \leq 0$ the relations are different. Already for small feedback gains the lead-lag eigen value becomes unstable, $G_\zeta = -0.21$. The flapping eigen value moves into the zero close to the torsion eigen value and the torsion eigen frequency increases to infinity.

The explanations demonstrate that the conclusions drawn from the signal flow diagram were right with respect to the sign of the feedback gains. If lag rate and lag attitude are both feed back towards the blade pitch control ϑ with $G_{\dot{\zeta}} \leq 0$ and $G_\zeta \geq 0$, lag damping can be increased without changing the lagging eigen frequency. The stiffening effect of the one feedback loop is canceled by the softening effect of the other. But, the decrease of flapping frequency may limit the feedback gains.

To optimize both feedback gains parallel output vec-

Eigen Values		
Open Loop	Output Vector Feedback	Full State Feedback
$-0.2744 \pm j3.132$	$-0.2770 \pm j3.131$	$-0.2783 \pm j3.130$
$-0.2035 \pm j1.136$	$-0.1913 \pm j1.100$	$-0.3041 \pm j1.133$
$-0.0027 \pm j0.670$	$-0.0472 \pm j0.667$	$-0.0579 \pm j0.672$

Feedback Gains		
Gain	Output Vector Feedback	Full State Feedback
$G_{\dot{\theta}}$	-	0.027
$G_{\dot{\beta}}$	-	0.492
$G_{\dot{\zeta}}$	-2.068	-3.159
G_{θ}	-	0.015
G_{β}	-	0.464
G_{ζ}	1.037	1.526

Table 3: Eigen Values and Feedback Gains

tor theory was applied [35]. Optimization of feedback gains was done with a computer program described in [36] applying optimal output vector theory [37]. A linear integral quadratic performance index is used which penalizes the entire state vector and control time history. Thus, every state may be penalized although only output variables are feed back

$$J = \int_0^\infty (\underline{x}^T \underline{Q} \, \underline{x} + \underline{u}^T \underline{R} \, \underline{u}) \, dt \; . \tag{28}$$

In the output feedback problem, the performance index is dependent on the initial conditions of the state vector and the weighting matrices $\underline{Q}$ and $\underline{R}$. In order to eliminate the dependence on the initial states the performance criterion is averaged for a linearly independent set of initial states. The control vector is defined as

$$\underline{u} = -\underline{G} \, y = -\underline{G} \, \underline{C} \, x \tag{29}$$

where $\underline{G}$ is the gain matrix and $\underline{C}$ the output matrix. Hence, the closed loop plant matrix becomes

$$\underline{A}_{cl} = \underline{A} - \underline{B} \, \underline{G} \, \underline{C} \; . \tag{30}$$

Optimization was performed such that two boundary conditions were not violated:

1. ω_β not below 1.1 and

2. $\Delta\vartheta_{max}$ below 2° for $\Delta\zeta(\psi = 0) = 1°$.

Parallel to the output vector optimization a full state feedback compensator was designed for the same boundary conditions. The comparison between the two control approaches and the open loop case is shown in fig. 7. The figure shows the BODE diagram for the transfer function from ϑ to ζ with the maximum of amplitude at the eigen frequency of the lead-lag motion. Output vector feedback results already

in an enormous reduction of $24dB$ in lead-lag amplitude and full state feedback of about $28dB$. The phase does not vary much between the three cases. Table 3 shows open and closed loop eigen values and the feedback gains.

Again, the signs of $G_{\dot{\zeta}}$ and G_ζ agree with the principle thoughts mentioned above. All feedback gains are small. The real part σ_ζ of both closed loop cases differs from the open loop values by a factor of about 17 for output vector feedback and 21 for full state feedback. This difference in both active control results is quite small, but can be explained with the boundary conditions. Whereas the first boundary condition is the limiting problem for the output vector concept the second condition is important for full state feedback. The flapping frequency is exactly 1.1 for lead-lag rate and attitude feedback and 1.133 for optimal control. This value is pretty close to the open loop value. The maximum control amplitude is 1.68° for output vector feedback and 2.0° for the full state controller. Of course, if weaker boundary conditions were chosen, more damping could be added to the lead-lag motion.

3.2 Lag Damping Augmentation in Forward Flight

To consider stability and active control of a helicopter in forward flight becomes more difficult than in hover for the system periodicity. This periodicity derives from the changing aerodynamic relations with rotor azimuth ψ that causes varying rotor loads. The periodicity's influence increases with increasing forward speed. As shown in fig. 3 the lead-lag damping has its minimum value at $\mu = 0.16$. This advance ratio was chosen for the root locus plot fig. 8. Feedback signals were once more both lead-lag states. But, this time the feedback gains were limited to certain values. Increasing the feedback gains beyond this causes a pair of complex conjugated eigen values to break up into two complex poles with the same magnitude of imaginary part but with different real parts. This behaviour is well known for periodic system equations [31] and can be easily seen from MATHIEU's equation. If lag rate (left hand side) is feed back the gain is limited to -33. For small gains the eigen values behave similar to fig. 6. With increasing gain this time the lead-lag mode becomes unstable for $G_{\dot{\zeta}} = -21.2$. The torsional mode does not change much within the given range of $G_{\dot{\zeta}}$. If lag attitude (right hand side) is feed back the relations are close to the hover results. Again, the lead-lag motion becomes unstable for negative gains at $G_\zeta = -0.18$. Comparing fig. 8 with fig. 6 this points out the possibility to augment lead-lag damping with one set of feedback gains within the whole flight regime. As long as the chosen feedback gains are small the actively controlled isolated rotor blade behaves similar in hover and in forward flight.

Finally, fig. 9 presents open and closed loop lead-lag damping in forward flight for different controller gains. Coming back to the conclusion drawn from both root locus plots the hover gains optimized with output vector theory ($G_{\dot\zeta} = -2.068$, $G_\zeta = 1.037$) were applied. Already this first crude approach results in sufficient lead-lag damping for all advance ratios, but the enormous stabilization in hover cannot be maintained within the speed range. The real part σ_ζ decreases from -0.0472 in hover to -0.0206 at $\mu = 0.17$ which is still 15 times the minimum open loop value at $\mu = 0.16$. The control effort stays well below $2°$. However, ω_β becomes smaller than 1.1 for $\mu > 0.34$. Optimizing the gains with forward speed considering only the first boundary condition achieves better damping levels than before. The obtained gains are shown on the left hand side of the figure. Both gains show the inverted nature of the lead-lag damping curve. That was to be expected. The real part σ_ζ does not drop as much as before, but the curve still has a minimum. For $\mu > 0.32$ the damping level is below that of the closed loop system using hover gains. If the control effort was plotted versus advance ratio, one could see the almost constant control amplitude $\Delta\vartheta_{max} \approx 1.7°$ for keeping the gains constant to the hover values. In contrast to that a maximum amplitude of $\Delta\vartheta_{max} = 3.3°$ at $\mu = 0.16$ for the variable gain case arises. Since the magnitudes of $G_{\dot\zeta}$ and G_ζ for $\mu > 0.32$ are smaller than the hover gains, the control amplitude drops below $1.7°$. With this the damping levels become worse than for the hover gain case.

If both boundary conditions are taken into account, the gains have to be limited within a certain speed range. These limits are marked by a dashed line in the left hand side of the figure. Due to the gain limitation for $0.05 < \mu < 0.305$ the lag damping diverges within this range from the variable gain curve to lower values. Both curves are identical for the remaining range of advance ratio.

These simple explanations demonstrate the simplicity to provide an isolated rotor with considerable lead-lag damping even in forward flight with lag rate and attitude feed back only. In the following section some facts shall be discussed that may limit the success of IBC to suppress ground or air resonance.

4 IBC to Suppress Ground Resonance

The spatial helicopter model for this part of the study is shown in fig. 10 and includes all six body DOFs. The rotor hub is located directly above the fuselage c.g. The blades are assumed to be rigid undergoing flapping and lagging motion rotating against linear spring and damper restraints. Lead-lag and flap motion have the same virtual hinge in common with a distinct offset a from the rotor centre. Structural flap-lag coupling, precone and linear twist can be in-

cluded. Aerodynamic rotor blade forces and moments are based on a linear two-dimensional blade element theory. Fuselage aerodynamics are included in the form of a linear derivative approach. Tail rotor dynamics are not modelled. A dynamic inflow model was not included although this is an important modelling aspect [16, 33]. The landing gear is represented by a system of linear springs and viscoelastic dampers at each of the four landing gear levers.

All differential equations were derived in a dimensional form by using the symbolic manipulation programs DERIVE and REDUCE, considering all geometric nonlinearities. These equations were included in a time integration routine to compute the time history results used later on. The system equations of motion were linearized to perform stability calculations. No ordering scheme was used this time, so all terms are retained in the analysis. A multiblade transformation was performed [31]. Assuming all blades to be identical and restricting the analysis to hover condition this results in 14 second order differential equations for body and rotor with constant coefficients. After a state space transformation one gets 28 first order differential equations. The data of the nominal configuration and further notations can be found in ref. [27].

Fig. 11 shows real and imaginary parts of the eigen values for the helicopter on ground. Thrust to weight ratio was set to $F/mg = 50\%$ and rotor speed was varied from 80% to $140\%\Omega_{nom}$. The eigen modes were identified at nominal rotor speed. The 28 states result in 14 complex conjugated values where fig. 10 includes only important eigen values. The figure clearly shows the curve for the regressing lead-lag motion of a soft inplane hingeless rotor helicopter whereas the frequency curve for the progressing lead-lag mode is not visible. The collective lead-lag mode couples with body yawing motion. Furthermore, the figure shows low frequency eigen modes for regressing flap. The eigen frequencies of body Θ/x and Φ/y modes result in a coalescence of the regressing lead-lag eigen frequency at 118% and $133\%\Omega_{nom}$, respectively. At these two points the regressing lead-lag mode couples with the body modes and new modes arise, two for each point of frequency coalescence. Whereas the one is stabilized the other is destabilized. In both cases an instability exists characterizing the ground resonance case. For clearness: it cannot be said whether the body mode or regressing lead-lag becomes unstable as can be read by several authors investigating ground and air resonance. The instability is caused by a coupling of eigen modes and one of the new coupled eigen modes becomes unstable.

Coming back to the results presented in [27] fig. 12 shows time history results with and without consideration of fuselage and both cases once open and once closed loop. Thrust to weight ratio was set to 50%,

F/mg	open loop		closed loop	
	ω_0 [rad/s]	D [%]	ω_0 [rad/s]	D [%]
0	32.7	2.85	32.7	2.12
10	32.7	2.85	32.2	4.00
50	32.7	2.91	31.4	8.03
100	32.7	3.02	30.6	12.03

Table 4: Damping Ratio and Eigen Frequency of the Isolated Rotor Blade

Mode	open loop		closed loop	
	ω_0 [rad/s]	D [%]	ω_0 [rad/s]	D [%]
ζ	32.4	-1.07	32.1	0.57
Θ/x	20.3	-1.71	20.8	1.38

Table 5: Damping Ratio and Eigen Frequency of Lead-Lag (Rotating System) and Body Pitch (Fixed System)

rotor speed to $118\%\Omega_{nom}$. This leads to a lag body pitch coupling. The lead-lag angle is given in the rotating frame. Optimization of feedback parameters was done with the fully nonlinear, coupled set of differential equations of motion by changing the feedback gains systematically and analyzing time history results. No numerical optimization algorithm was used. In addition to the studies presented in section 3 lag acceleration was fed back.

Since it was meant to be favourable to increase lead-lag damping of an isolated rotor blade, the impact of blade motions on the fuselage was neglected first. This was done by switching off the body degrees of freedom. The idea was that mechanical lead-lag dampers add damping to an isolated blade, too. To optimize such a damper the fuselage does not need to be considered. The both time history results at the top of the figure show that lead-lag damping can be easily increased with these three feedback loops. The feedback gains are given in the figure, too. They were chosen such that lead-lag damping was maximized, but an excitation of the flapping motion was avoided. The signs of lead-lag rate and attitude feedback agree with those of the previous section. Table 4 includes eigen frequency ω_0 and damping ratio D of the open and closed loop system for various thrust to weight ratios F/mg. Damping ratios and eigen frequencies were computed from time history results. The damping ratio of 2.91% at 50% airborne for the isolated blade without feedback is not sufficient to avoid ground resonance. One closing the feedback loops with the given gains, the damping ratio increases to 8.03%. This value achieved by mechanical lead-lag dampers would be sufficient to avoid ground resonance. Table 4 also shows that with increasing thrust the damping results get better. But at zero thrust the optimized gains slightly reduce closed loop lag damping. Since aerodynamic forces and moments at the rotor blade increase with thrust, i.e. collective pitch, aerodynamics should not be neglected in the controller design process as done in [24]. Including fuselage motion, however, the feedback gains determined for the isolated blade even increase instability (fig. 12 lower top). This result is quite astonishing, since it disproves the idea of optimizing an IBC system for the isolated blade. This becomes clear, if one considers that the fuselage motions are inputs for the rotor calculation and vise versa.

Finally, a controller was designed for ground resonance damping. During the design process several restrictions were found out. First, none of the feedback loops could stabilize the system without the others. Secondly, lag rate and lag attitude feedback gains were limited, because of an excitation of the flapping motion. This flap excitation reduces closed loop system damping. The time history results and feedback gains are shown in fig. 12 (bottom). This time the rotor body system can be stabilized, whereas the isolated blade is destabilized. As can be seen $G_{\dot\zeta}$ and G_{ζ} differ in sign from that of the previous controller. Table 5 shows open and closed loop damping for the rotor body system. At least, fig. 13 compares the open loop time history results of the isolated rotor blade to that of the rotor body system for $50\%F/mg$ and $118\%\Omega_{nom}$. An initial lead-lag disturbance of $0.5°$ was applied to excite the system. Whereas the lead-lag motion of the isolated rotor blade is a damped harmonic oscillation, the lead-lag angel of the rotor-body system shows a more irregular character. After the transient response vanished, the oscillations slightly increase and depict a self-excited oscillation. A certain time step is marked with arrows. While the lagging motion of the isolated blade shows a local minimum at this time step the lead-lag angle of the coupled rotor body system shows a local maximum. This means a phase shift of $180°$ at this point. From this it becomes clear that body dynamics must not be neglected for an IBC design to suppress ground resonance.

The control results indicate that ground resonance stability can be improved through the use of IBC, but the consideration of an isolated blade is not feasible. Compared to an SAS approach the results are poor [7, 15, 27].

5 Outlook and Conclusion

The intent of the presented investigation was to demonstrate the possibilities of active control to augment rotor lead-lag damping in hover and forward flight and to provide an insight into the behaviour of the actively controlled rotor.

First, the study dealt with the consideration of an isolated rotor blade in forward flight. A three degree of freedom flap-lag-torsion model was derived. The equations of motion were linearized. FLOQUET theory was

used to compute characteristic multipliers and from that the eigen values. The isolated rotor blade showed a minimum damping at $\mu = 0.16$. From that simple model the following conclusions can be drawn:

- augmentation of lead-lag damping is possible with simple ζ- and $\dot{\zeta}$-feedback without a significant manipulation of rotor dynamics and high control effort,

- root locus plots show almost the same trends in hover and forward flight for low $G_{\dot{\zeta}}$- and G_{ζ}-gains,

- simple controller design for the whole range of advance ratio seems to be possible without scheduling of feedback gains.

Secondly, a fully spatial helicopter model for ground resonance studies was used to examine active control and to guarantee aeromechanical stability with an IBC approach. The model included flap and lead-lag for each rotor blade and all six body DOFs. From that model it became clear that fuselage DOFs have to be taken into account for the design of an active control device.

Regarding this it becomes obvious that further systematic studies have to be carried out in order to explore the full potential of active control of aeromechanical instabilities and to investigate the impact of active control on the dynamic behaviour of a helicopter. Further work should:

- consider more sophisticated models with elastic blade deflections and fuselage DOFs to avoid adverse effects on helicopter dynamics,

- include actuator and sensor dynamics to the feedback loop for realistic controller designs and

- compare IBC to other controller designs that use multiblade or fuselage states as feedback signals.

Acknowledgements

References

[1] G. Reichert, H. Huber. Influence of elastic coupling effects on the handling qualities of a hingeless rotor helicopter. *AGARD CP - 121*, pages 8.1 – 8.15, February 1973.

[2] H. Huber. Effect of torsion-flap-lag coupling on hingeless rotor stability. *29th Annual National Forum of the American Helicopter Society*, pages 1–14, May 1973.

[3] R.E. Hansford, I.A. Simons. Torsion-flap-lag coupling on helicopter rotor blades. *Journal of the American Helicopter Society*, 18(4):2 – 12, October 1973.

[4] R.E. Donham, S.V. Cardinale, I.B. Sachs. Ground and air resonance characteristics of a soft in-plane rigid-rotor system. *Journal of the American Helicopter Society*, 14(4):33 – 41, October 1969.

[5] R.A. Ormiston. Aeromechanical stability of soft inplane hingeless rotor helicopters. *3rd European Rotorcraft Forum*, Aix-En-Provence, France, pages 25.1 – 25.22, September 7 – 9 1977.

[6] R.T. Lytwyn, W. Miao, W. Woitsch. Airborne and ground resonance of hingeless rotors. *Journal of the American Helicopter Society*, 16(2):2 – 9, April 1971.

[7] Ch. Kessler, G. Reichert. Active control of ground and air resonance including transition from ground to air. *20th European Rotorcraft Forum*, Amsterdam, Netherlands, pages 64.1 – 64.17, October 4 – 7 1994.

[8] D.A. Peters. Flap-lag stability of helicopter rotor blades in forward flight. *Journal of the American Helicopter Society*, 20(4):1 – 13, 1975.

[9] B. Panda, I. Chopra. Flap-lag-torsion stability in forward flight. *Journal of the American Helicopter Society*, 30(4):30 – 39, October 1985.

[10] D.H. Hodges, R.A. Ormiston. Stability of elastic bending and torsion of uniform cantilever rotor blades in hover with variable structural coupling. *NASA TN D-8192*, April 1976.

[11] R.A. Ormiston, W.G. Warmbrodt, D.H. Hodges, D.A. Peters. Rotorcraft aeroelastic stability. *NASA CP-2495*, pages 353–529, 1988.

[12] G. Reichert. Active control of helicopter ground and air resonance. *3rd Technical Workshop: Dynamics and Aeroelastic Stability Modeling of Rotorcraft Systems*, Duke University, Durham, North Carolina, March 12 – 14 1990.

[13] M.I. Young, D.J. Bailey, M.S. Hirschbein. Open and closed loop stability of hingeless rotor helicopter air and ground resonance. *AHS/NASA-Ames Specialists' Meeting on Rotorcraft Dynamics*, pages 1 – 32, February 13 – 15 1974.

[14] F.K. Straub, W. Warmbrodt. The use of active controls to augment rotor/fuselage stability. *Journal of the American Helicopter Society*, 30(3):13 – 22, July 1985.

[15] F.K. Straub. Optimal control of helicopter aeromechanical stability. *11th European Rotorcraft Forum*, London, England, pages 77.1 – 77.16, September 10 – 13 1985.

[16] M.D. Takahashi, P.P. Friedmann. A model for active control of helicopter air resonance in hover and forward flight. *14th European Rotorcraft Forum*, Milano, Italy, pages 57.1 – 57.23, September 20 – 23 1988.

[17] R. Kube, B.v.d. Vall, K.-J. Schultz. Mechanisms of vibration and BVI noise reduction by Higher Harmonic Control. *20th European Rotorcraft Forum, Amsterdam, Netherlands*, pages 27.1 – 27.23, October 4 – 7 1994.

[18] P. Richter, T. Schreiber. Theoretical Investigations and wind-tunnel tests with HHC-IBC. *20th European Rotorcraft Forum*,Amsterdam, Netherlands, pages 71.1 – 71.15, October 4 – 7 1994.

[19] N.D. Ham. Helicopter Individual Blade Control and its applications. *9th European Rotorcraft Forum*, Stresa, Italy, pages 56.1 – 56.11, September 13-15 1983.

[20] N.D. Ham. A simple system for helicopter Individual Blade Control using modal decomposition. *Vertica*, 4(1):23 – 28, 1980.

[21] N.D. Ham. Helicopter Individual Blade Control research at MIT 1977-1985. *Vertica*, 11(1/2):109 – 122, 1987.

[22] N.D. Ham, T.R. Quackenbush. A simple system for helicopter individual-blade-control and its application to stall flutter suppression. *7th European Rotorcraft Forum*, Garmisch-Partenkirchen, Germany, pages 76.1 – 76.28, September 8 – 11 1981.

[23] N.D. Ham. Helicopter gust alleviation, attitude stabilisation, and vibration alleviation using individual-blabe-control through a conventional swash plate. *11th European Rotorcraft Forum*, London, England, pages 75.1 – 75.5, September 10 – 13 1985.

[24] N.D. Ham, B.L. Behal, R.M. McKillip. Helicopter rotor lag damping augmentation through individual-blade-control. *Vertica*, 7(4):361 – 371, 1983.

[25] D.Teves, V. Kl"oppel, P. Richter. Development of active control technology in the rotating system, flight testing and theoretical investigation. *19th European Rotorcraft Forum*,Avignon, France, pages 89.1 – 89.13, September 15 – 18 1992.

[26] P. Richter, A. Blaas. Full sacle wind tunnel investigation of an individual blade control system for Bo 105 hingeless rotor. *19th European Rotorcraft Forum*, Cernobbio (Como), Italy, pages G5.1 – G5.12, September 14 – 16 1990.

[27] G. Reichert, U. Arnold. Active control of helicopter ground and air resonance. *16th European Rotorcraft Forum*, Glasgow, Scotland, pages III.6.2.1 – III.6.2.14, September 18 – 20 1990.

[28] P.P. Friedmann. Helicopter rotor dynamics and aeroelasticity: Some key ideas and insights. *Vertica*, 14(1):101–121, 1990.

[29] R.A. Ormiston, D.H. Hodges. Linear flap-lag dynamics of hingeless helicopter rotor blades in hover. *Journal of the American Helicopter Society*, 17(2):2 – 14, April 1972.

[30] M.D. Takahashi. *Active control of helicopter aeromechanical and aeroelastic instabilities*. Dissertation, University of California, Los Angeles, 1988.

[31] W. Johnson. *Helicopter Theory*. Princeton University Press, 1980.

[32] B. Panda, I. Chopra. Flap-lag-torsion stability in forward flight. *2nd Decennial Specialists' Meeting on Rotorcraft Dynamics*, NASA Ames Research Center, Moffet Field, California, pages 241 – 258, November 7 – 9 1984.

[33] H.C. Curtiss Jr. Stability and control modelling. *Vertica*, 12(4):381 – 394, 1988.

[34] M.A. Diftler. UH 60A helicopter stability augmentation study. *14th European Rotorcraft Forum*, Mailand, Italy, pages 74.1 – 74.15, September 20 – 23 1988.

[35] O. Föllinger. Entwurf konstanter Ausgangsrückführungen im Zustandsraum. *Automatisierungstechnik*, 34(1):5 – 15, Januar 1986.

[36] M.E. Wasikowski. *Optimal Output Vector Feedback, Theory Manual*. Georgia Tech Research Institute, Atlanta, Georgia, 1992.

[37] W.S. Levine, M. Athenas. On the determination of the optimal constant output feedback gains for linear multivariable systems. *IEEE Transactions on Automatic Control*, 15(1):44 – 48, February 1970.
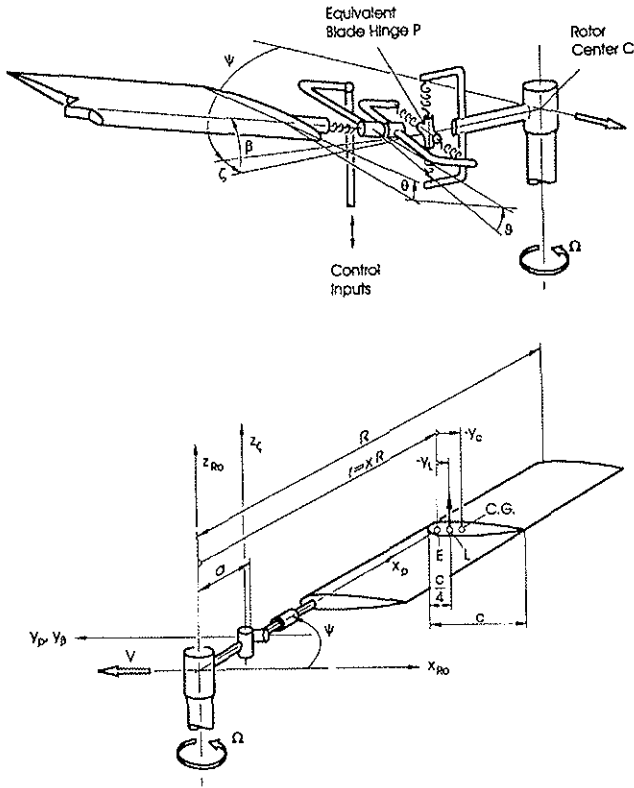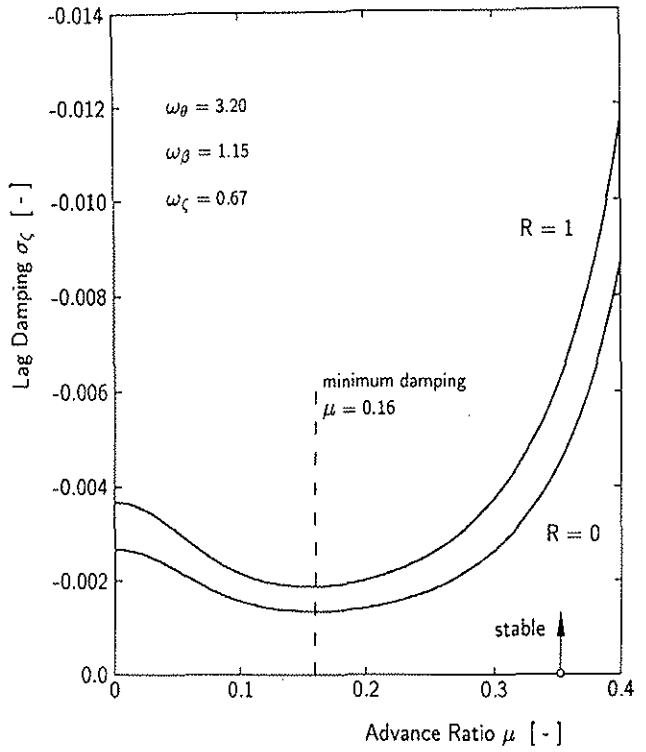
Figure 1: Rotor Blade Model and Blade Geometry

Figure 2: Propulsive Trim Solution vs. Advance Ratio
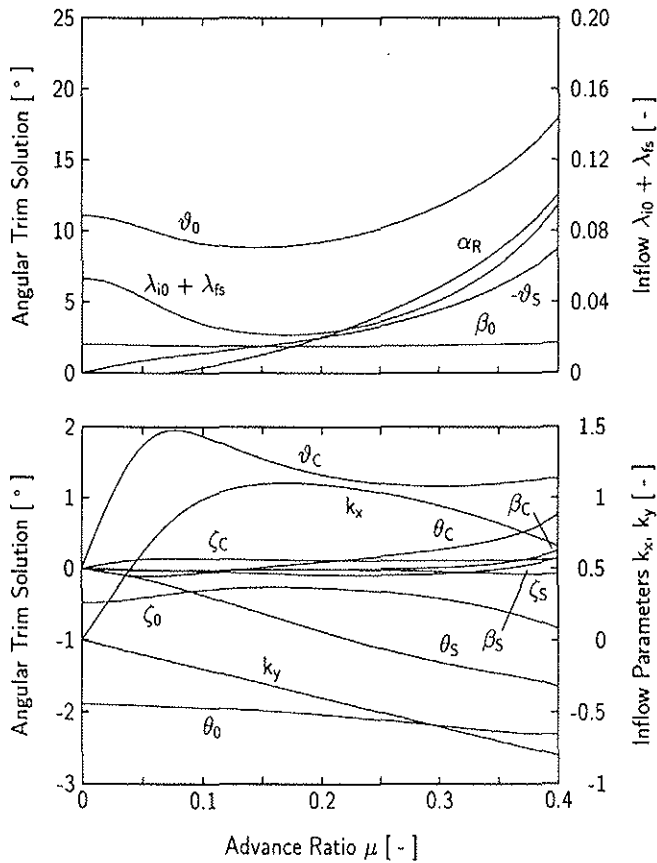

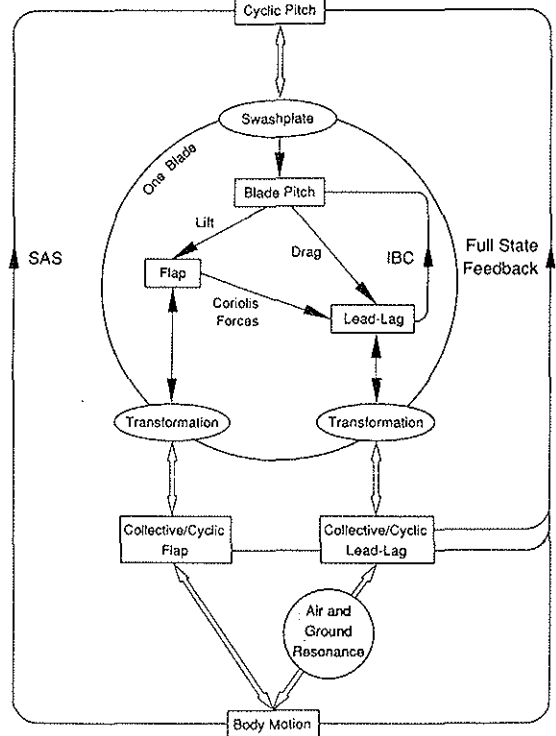Figure 3: Lag Damping vs. Advance Ratio

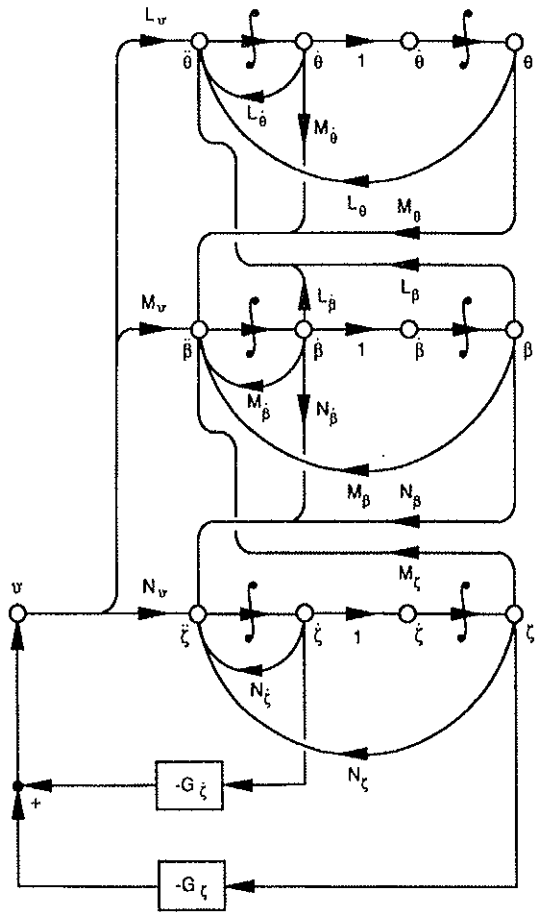Figure 4: Active Control Concepts to Augment Rotor-Body Stability

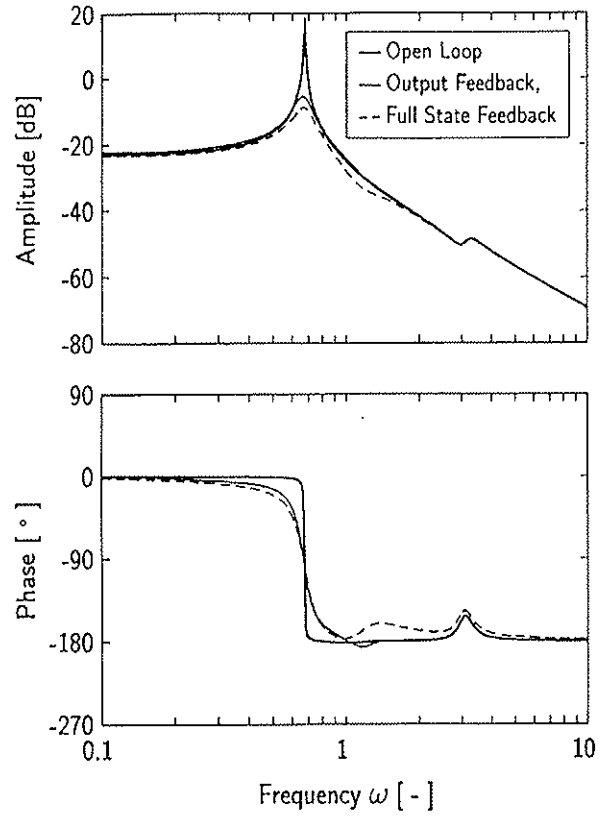Figure 5: Signal Flow Diagram of Isolated Rotor Blade in Hover

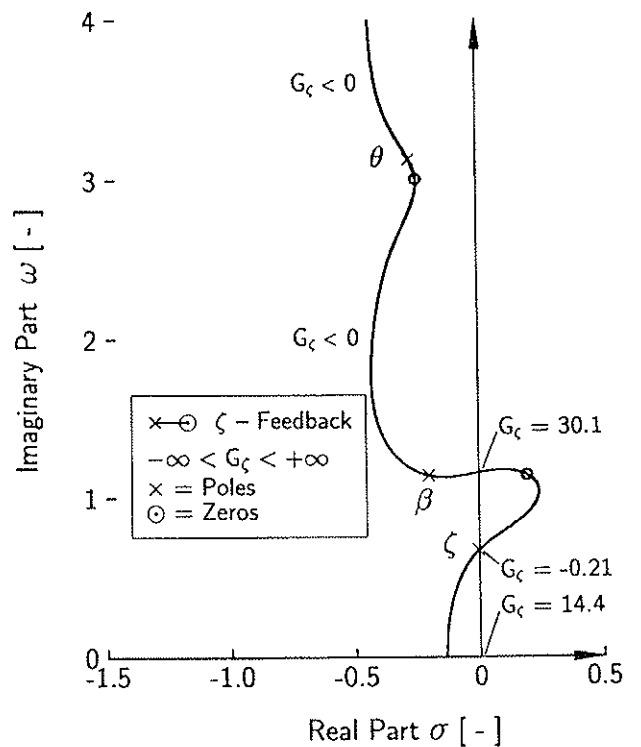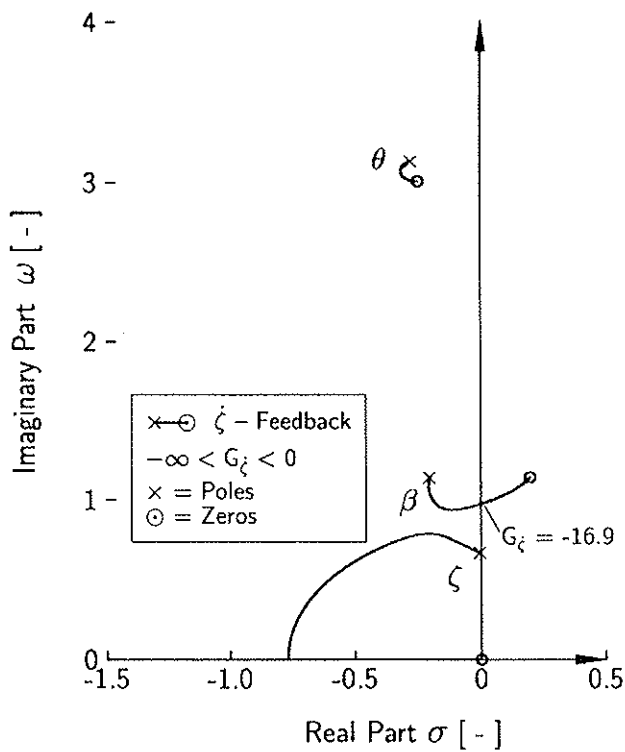Figure 7: Bode Diagram for Transfer from Control Input to Lead-Lag Angle $\mu=0$, R=0

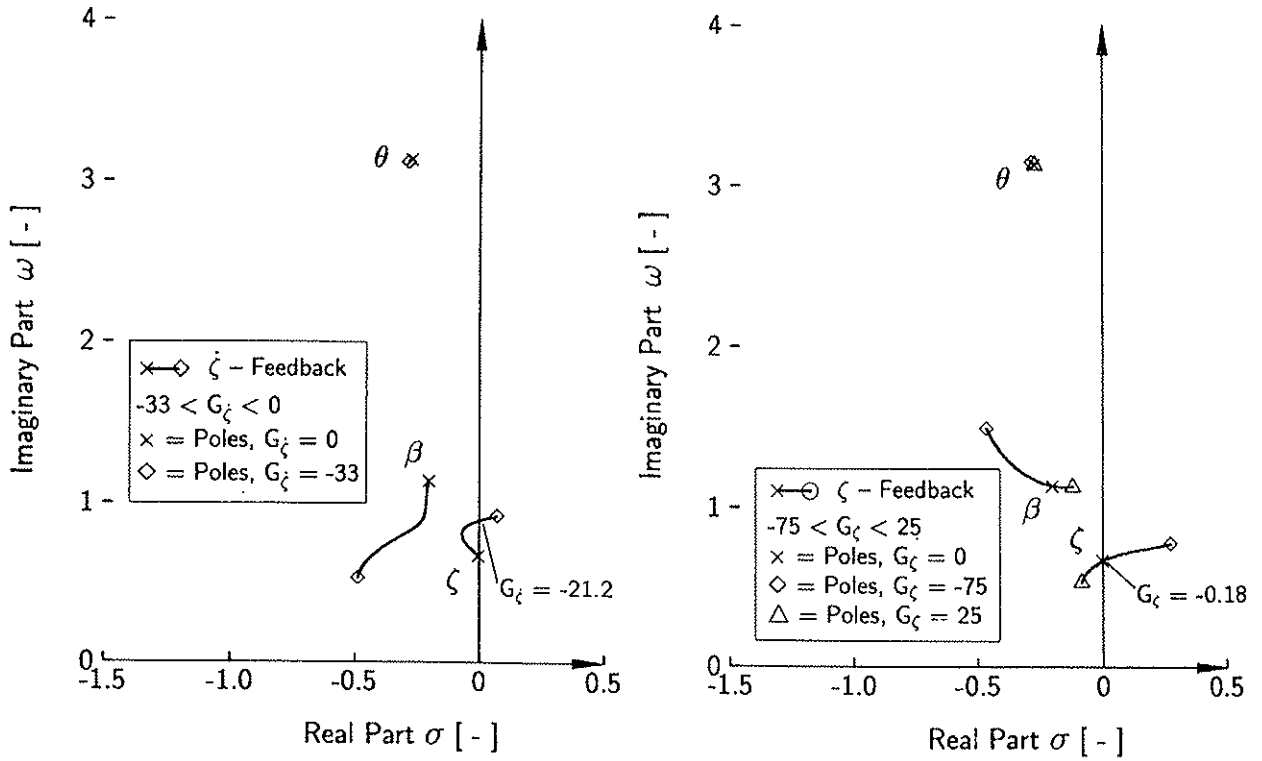Figure 6: Root Locus for Lead-Lag-State Feedback, $\mu=0$, R=0

Figure 8: Root Locus Lead-Lag-State Feedback, μ=0.16, R=0
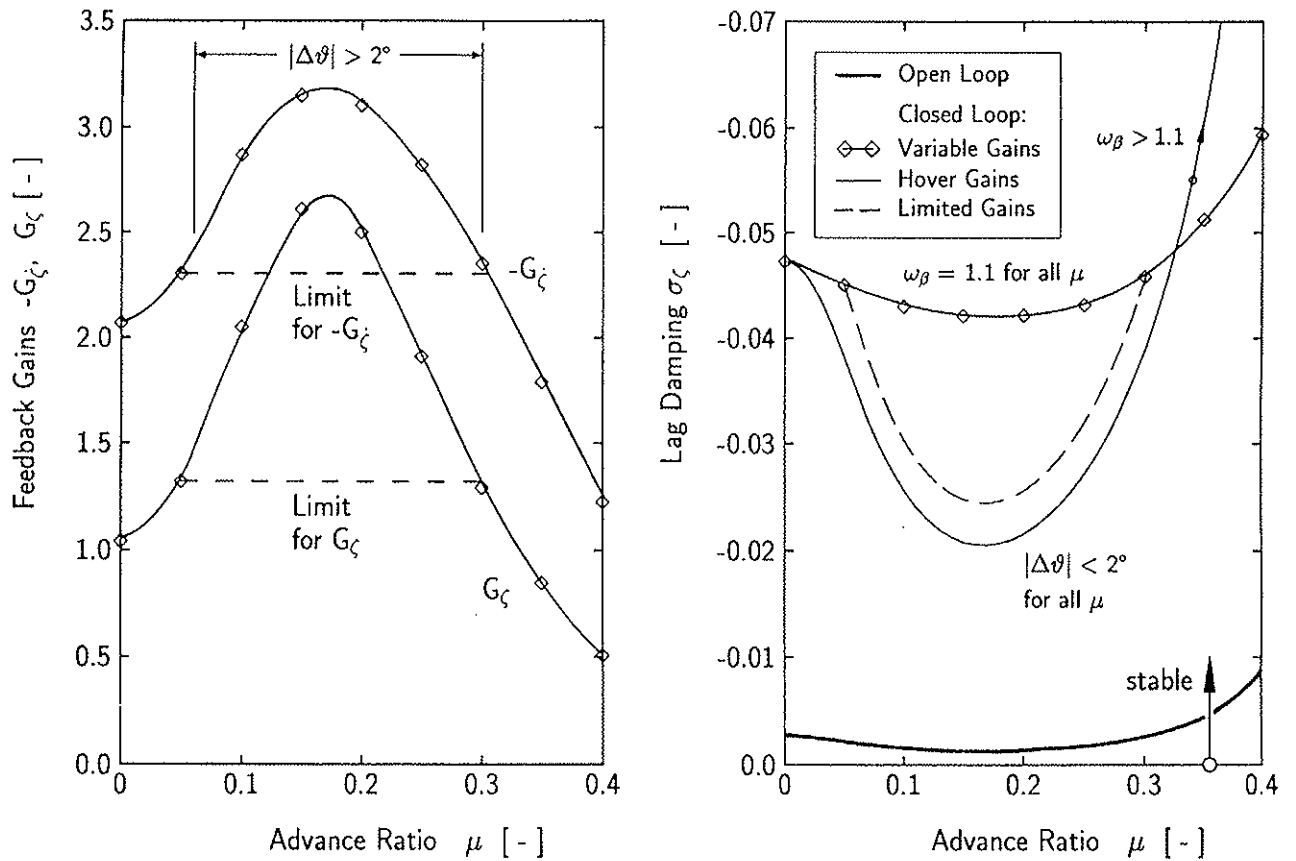
Figure 9: Feedback Gains and Lag Damping vs. Advance Ratio, R=0
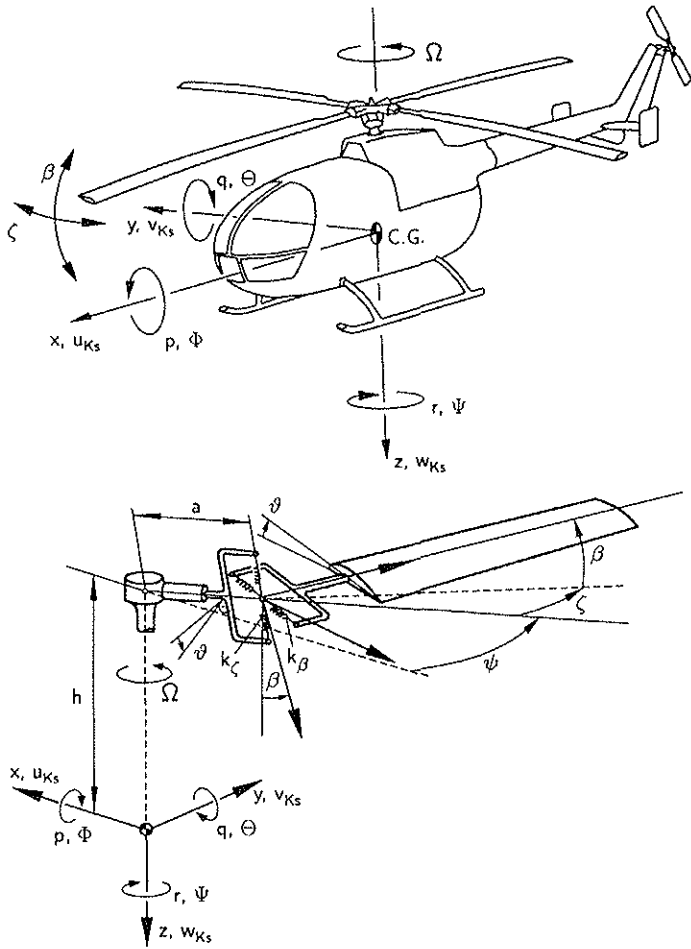
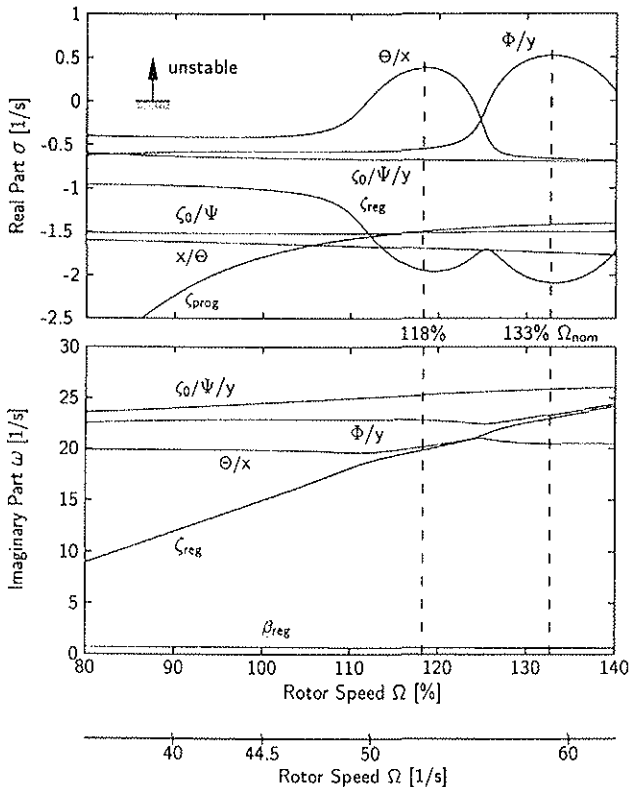Figure 10: Mathematical Helicopter Model Used by REICHERT and ARNOLD

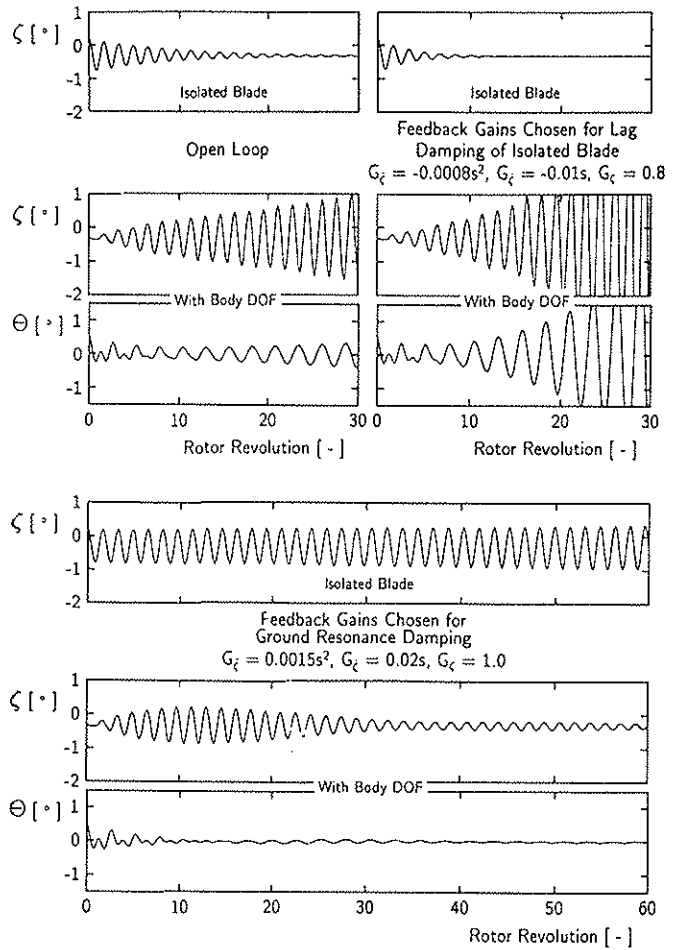Figure 11: Eigen Values of the Coupled Rotor-Body-System on Ground, F/mg=50%

Figure 12: Lag Damping Augmentation through IBC, Isolated Blade Compared with Helicopter on Ground, 118% Ω_{nom}, F/mg=50%
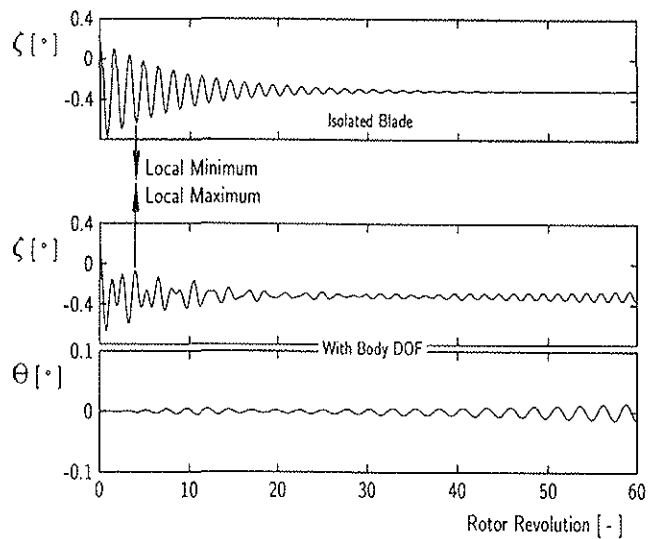

Figure 13: Open Loop Lead-Lag Response of Isolated Blade Compared with Helicopter on Ground, 118% Ω_{nom}, F/mg=50%